Geophysical Journal International

Geophys. J. Int. (2016) **205,** 1290–1304
Advance Access publication 2016 February 24
GJI Gravity, geodesy and tides

doi: 10.1093/gji/ggw078

Five years' gravity observation with the superconducting gravimeter OSG#058 at Syowa Station, East Antarctica: gravitational effects of accumulated snow mass

Yuichi Aoyama,[1] Koichiro Doi,[1] Hiroshi Ikeda,[2] Hideaki Hayakawa[3] and Kazuo Shibuya[3]

[1]*National Institute of Polar Research and SOKENDAI,* 10-3 *Midori-cho, Tachikawa, Tokyo* 190–8518, *Japan. E-mail: aoyama@nipr.ac.jp*
[2]*Research Facility Center for Science and Technology, Cryogenics Division, University of Tsukuba, Tsukuba, Ibaraki* 305–8577, *Japan*
[3]*National Institute of Polar Research,* 10-3 *Midori-cho, Tachikawa, Tokyo* 190–8518, *Japan*

Accepted 2016 February 22. Received 2016 February 18; in original form 2015 December 23

SUMMARY

Continuous gravimetric observations have been made with three successive generations of superconducting gravimeter over 20 yr at Syowa Station (39.6°E, 69.0°S), East Antarctica. The third-generation instrument, OSG#058, was installed in January 2010 and was calibrated by an absolute gravimeter during January and February, 2010. The estimated scale factor was -73.823 ± 0.053 μGal V^{-1} (1 μGal $= 10^{-8}$ m s^{-2}). The first 5 yr of OSG#058 data from 2010 January 7 to 2015 January 10 were decomposed into tidal waves (M3 to Ssa) and other non-tidal components by applying the Bayesian tidal analysis program BAYTAP. Long-term non-tidal gravity residuals, which were obtained by subtracting annual and 18.6 year tidal waves and the predicted gravity response to the Earth's variable rotation, showed significant correlation with the accumulated snow depth measured at Syowa Station. The greatest correlation occurred when the gravity variations lagged the accumulated snow depth by 21 d. To estimate the gravitational effect of the accumulated snow mass, we inferred a conversion factor of 3.13 ± 0.08 μGal m^{-1} from this relation. The accumulated snow depth at Syowa Station was found to represent an extensive terrestrial water storage (the snow accumulation) around Syowa Station, which was estimated from the Gravity Recovery and Climate Experiment satellite gravity data. The snow accumulation around Syowa Station was detectable by the superconducting gravimeter.

Key words: Time-series analysis; Satellite geodesy; Time variable gravity; Antarctica.

1 INTRODUCTION

The Antarctic ice sheet is a huge heat sink that acts as a feedback controller for adjusting global warming. Monitoring changes in its mass is important in predicting global environmental change. In recent decades, these estimations have been made using satellite observations such as radar/laser altimetry, synthetic aperture radar, and gravity mission satellites (e.g. Chen *et al.* 2006; Velicogna & Wahr 2006; Rignot *et al.* 2008; Chen *et al.* 2009; Rignot *et al.* 2011; Shepherd *et al.* 2012). The satellite mission of the Gravity Recovery and Climate Experiment (GRACE) observes temporal and spatial variations in the Earth's gravitational field; these changes reflect redistributions of the Earth's surface mass (Tapley *et al.* 2004). Unlike other satellite observations, GRACE can detect surface mass changes directly, and is useful for the estimation of terrestrial water storage (including ice masses on the land). GRACE data have provided evidence of increasing surface ice mass in East Antarctica (e.g. Shepherd *et al.* 2012), especially in the coastal region of Dronning Maud Land (DML; at longitudes from 20°W to 44.6°E) since 2009 (Boening *et al.* 2012; Shepherd *et al.* 2012). Several studies have attributed the mass increase to increased snowfall in the region (Boening *et al.* 2012; Lenaerts *et al.* 2013).

In contrast, Chen *et al.* (2009) reported that GRACE data showed an acceleration in the loss of ice mass, even in East Antarctica, since 2006. This apparent conflict with the findings of other studies may be partly attributed to the error (uncertainty) in the glacial isostatic adjustment (GIA) models (Chen *et al.* 2009). Clarification can be gained by comparing the satellite observations with the corresponding ground gravity measurements.

Syowa Station, the main wintering station of the Japanese Antarctic Research Expedition (JARE), is located on East Ongul Island, DML, East Antarctica (Fig. 1). Several measurements with space-geodetic techniques such as Very Long Baseline Interferometry (VLBI), Global Navigation Satellite System (GNSS) and Doppler Orbitography and Radiopositioning Integrated by Satellite (DORIS) have been carried out since the 1990s to monitor crustal movements

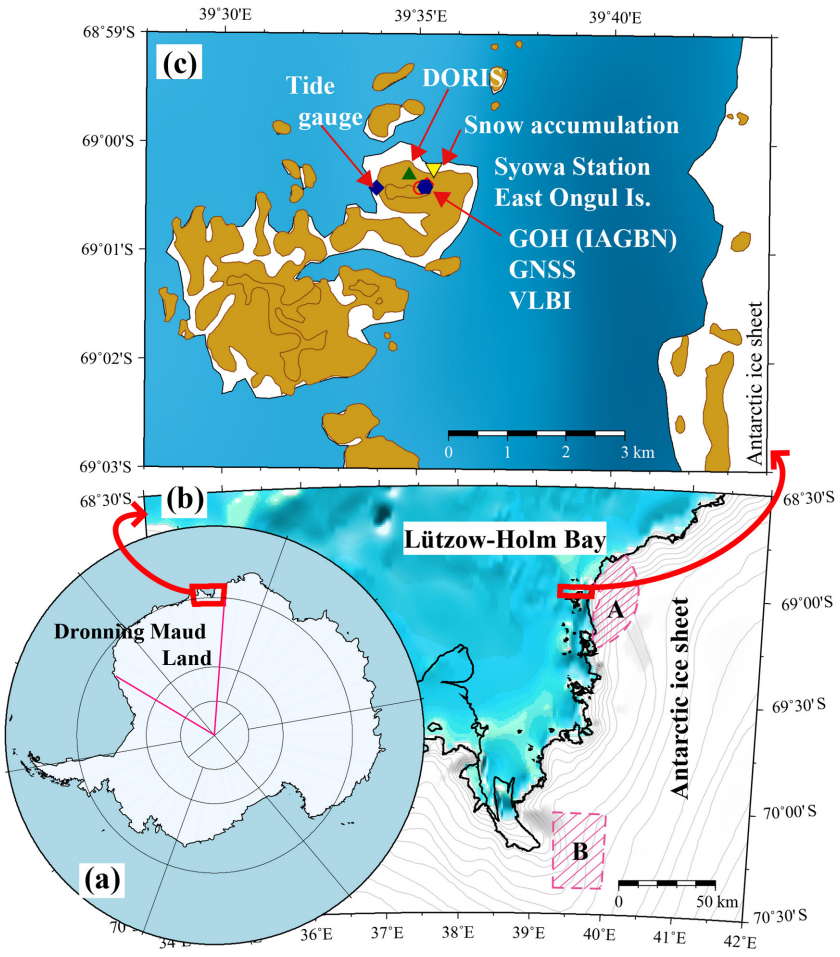

Figure 1. Location of Syowa Station, Ongul Island, in Dronning Maud Land, East Antarctica. (a) Map of whole Antarctica. Pink lines show boundaries of Dronning Maud Land. (b) Map of the coastal region of Lützow–Holm Bay. Pink shaded parts labelled A and B are areas where influences of accumulated snow mass to a gravity measurement at Syowa Station are estimated in Section 4.4. (c) Map of East Ongul Island. Continuous gravity measurements have been performed with superconducting gravimeters at Gravity Observation Hut (GOH).

in the region of Syowa Station and to contribute global geodetic measurement networks, while tide-gauge measurement has been performed since 1979 (Shibuya *et al.* 2005). In addition, the absolute gravity base in the Gravity Observation Hut (GOH) at Syowa Station is established as site number #0417 within the International Absolute Gravity Basestation Category A Network, hereafter termed the IAGBN(A)#0417 base (Shibuya *et al.* 2005). JARE has conducted continuous gravity observations with a superconducting gravimeter (SG) (also in the GOH) since 1993 (Shibuya *et al.* 2005).

To complement the geodetic observations, meteorological data have been recorded regularly since 1957 by the Japan Meteorological Agency, and are available from http://www.data.jma.go.jp/antarctic/datareport/01_sfc_synop/sfc_synop.html. The operational measurement of accumulated snow depth started in 1999; we use these data in this work to interpret the non-tidal gravity components in the SG records.

With the objective of evaluating changes in surface mass around DML, which are considered to occur on a timescale of decades, we use 5 yr of SG data (2010–2014) to deduce the gravitational effect of snow accumulation and GIA effect. We first verify 5 yr's observation by the third-generation SG at Syowa Station and reduce known gravity variations with tidal periods (Section 2). The decomposed tidal components are compared with those derived from 10 yr of SG (the first-generation SG) data in order to access its accuracy (Section 3). We infer influences of long-period variations in the Earth's surface mass by the atmosphere, ocean and snow (Section 4.1). The deduced long-term non-tidal gravity variation is compared with the daily data set of *in-situ* accumulated snow depth and the gravitational effect of the snow accumulation is estimated by an admittance method (Section 4.2). The estimate of the gravitational effect of the snow accumulation is evaluated by considering a simple attractive force of hollow-cylinder-shaped snow mass (Section 4.3). We compare the deduced long-period gravity variations with the GRACE-derived gravity variation in the region concerned, and validate the recent change in surface mass associated with snow accumulation in DML (Section 4.4). Our conclusions are described in Section 5.

2 SG OBSERVATIONS IN SYOWA STATION AND THEIR DATA ANALYSES

Gravity variations recorded by SGs at ground stations have already been compared with GRACE-derived gravity variations in Europe (e.g. Neumeyer *et al.* 2008; Weise *et al.* 2009; Crossley *et al.* 2012). Here we use continuous SG data obtained at Syowa Station to evaluate the recent surface mass change around DML derived from the GRACE data. For over 20 yr, three successive generations of SG

(TT-70#016, CT#043, and OSG#058) installed in the GOH (Fig. 1c) have recorded continuous gravity data with high precision and temporal resolution (Aoyama *et al.* 2015). We extract long-period gravity variations from the first 5 yr of OSG#058 data during 2010 January 7–2015 January 10 by subtracting components attributed to Earth and ocean tides, polar motion, atmospheric mass loading and short-period irregular noise. We infer the source of the non-tidal long-period variations using *in-situ* meteorological data. In addition, these decade-scale ground gravity variations are directly compared with GRACE-derived gravity variations.

2.1 Continuous SG observation of gravity variations

The first-generation SG (TT–70#016, with a 10 K cryocooler) started continuous gravity observation on 1993 March 22 (Sato *et al.* 1995). The data provided many results related to the Earth's tides, free oscillations and variable rotations in addition to seasonal variations in the ocean, whose magnitudes ranged from 0.001 to 100 μGal (1 μGal $= 10^{-8}$ m s^{-2}) (e.g. Sato *et al.* 1997; Nawa *et al.* 1998; Sato *et al.* 2001; Iwano *et al.* 2005; Kim *et al.* 2011). However, there was uncertainty in these deduced long-period gravity variations due to the significant step-like perturbations that arose in this instrument as a result of regular maintenance, during which gas helium was liquefied by a separate liquefier system and the obtained liquid helium (LHe) was transferred into the dewar of the TT–70#016 when the LHe levels become depleted (for details, see Appendix).

At the end of 2003, the TT–70#016 was replaced by a second-generation CT#043 with a 4.2 K cryocooler (Leybold Vacuum Products Inc., Germany); for further details, see Ikeda *et al.* (2005) and Doi *et al.* (2008). Although this instrument could liquefy gas helium inside dewar (without necessity of transferring LHe), its gravity data were contaminated by instrumental drift (Doi *et al.* 2008), and its isolation diaphragm could not prevent the passage of outside air into the dewar, resulting in the deposition of solidified air around the neck of the dewar. Since 2006, vibration from the cryocooler had propagated through the solidified air to the SG sensing unit, disturbing the gravity signals. Therefore, a third-generation OSG#058 with a 4.2 K cryocooler (Sumitomo Heavy Industries, Ltd., Japan) was installed on 2010 January 6 (for details of the installation, see Ikeda *et al.* 2011).

The integrated electronics of the OSG#058 include controlling modules for the gravimeter, temperature, and tilt, and the data acquisition system has a GPS clock, barometer, temperature and humidity sensors connected to a large uninterrupted power supply. These features have enabled continuous gravity measurement for over 5 yr without interruption, although sporadic power failures have disturbed other observations. Given the high quality and stability of the data, we will analyse and discuss the long-period gravity variations using data from 2010–2015, despite the limited data span of 5 yr.

2.2 Calibration of OSG#058

Inside the SG sensing unit, a hollow niobium sphere levitates in a steady magnetic field induced by a permanent electrical current flowing in the superconducting coils. The position of the sphere fluctuates only with variations in the gravitational field. The SG controls the position of the sphere via a magnetic feedback coil to maintain it in a fixed position against the gravitational force, and outputs a time-series of the voltage through the feedback coil. The feedback voltage is linearly proportional to the gravitational variation, and thus can provide a time-series of the gravitational variations via the application of a scale factor (units μGal V^{-1}).

The scale factor is generally determined by comparing the SG feedback voltages with simultaneous absolute gravity observations. During the installation period of OSG#058, a JARE member from the Geospatial Information Authority of Japan (hereafter referred to as GSI) performed absolute gravity measurements in the GOH with two absolute gravimeters, FG–5 #104 and #203 (Sugawara 2011). The time-series of simultaneous SG feedback voltages and absolute gravity observations are shown in Fig. 2(a). The FG–5 #104 and #203 were operated on the IAGBN(A)#0417 base and the adjacent spare base alternately.

From 2009 December 23 to 2010 February 9, FG–5 #104 and #203 respectively observed 142 494 and 128 367 total effective single drops. The observations were practically equivalent (Sugawara 2011), so that it was not necessary to distinguish between the data sets observed at the IAGBN(A)#0417 base and at the spare base. Consequently, after subtracting the median value of 982 524 327.5 μGal, which was consistent with the measured absolute gravity determined by GSI to within a range of ± 1.5 μGal, the residuals were compared with the SG data (Fig. 2b). The scale factors are estimated via linear regression (straight line fitting) by least trimmed squares regression, as applied by Rousseeuw & Van Driessen (2006). Fig. 2 exhibits that dispersion of the gravity observables from FG–5#203 is smaller than that from FG–5#104. Accordingly, an estimated slope of the straight line derived from FG–5 #203 is employed as the scale factor, which is -73.823 ± 0.053 μGal V^{-1}; its precision (0.07 per cent) for converting the SG feedback voltage to gravity is better than those (0.11 per cent and 0.13 per cent for TT–70#016 and CT#043, respectively) previously obtained by Iwano *et al.* (2003) and Doi *et al.* (2008).

2.3 Preprocessing data from OSG#058

The data acquisition system of OSG#058 provides seven daily data files: (1) gravity (SG feedback voltage) and barometer raw data at 1 s intervals; (2) auxiliary data such as room temperature, temperatures inside the dewar, tilt compensation status, and refrigeration system status, at 1 min intervals; (3 and 4) filtered and re-sampled raw data, at 10 s and 1 min intervals, respectively; (5) theoretical gravity values and gravity residuals at 1 min intervals; (6) comments and log; and (7) the system generated log. These daily files are automatically transferred daily to the National Institute of Polar Research (NIPR) by an FTP protocol via an INTELSAT satellite link. After receiving all the daily data files at NIPR, the gravity and barometer raw data and some auxiliary data in the above (1), (2), (4) and (5) data sets are graphed automatically. The daily graphs are automatically uploaded to the NIPR web server every day at 01 UTC, and are publicly accessible (Aoyama *et al.* 2015).

Fig. 3 shows gravity and dominant auxiliary data at 1 min intervals for the period 2010 January 6–2014 December 31. It is remarkable that only ∼4 per cent of the LHe had evaporated over the 5 yr (Fig. 3i), an average of 0.8 per cent per year, and much less than the evaporation rates of the previous two SGs. The reduced rate is attributable to the new diaphragm of the OSG#058, which isolates the gravity sensor from vibrations arising from the cold-head of the cryocooler, thus preventing the leakage of any helium gas from within (Ikeda *et al.* 2011). A sharp decrease of 2.8 per cent (indicating a rapid evaporation of LHe) in February 2012 occurred during replacement of the coldhead; however, there was no

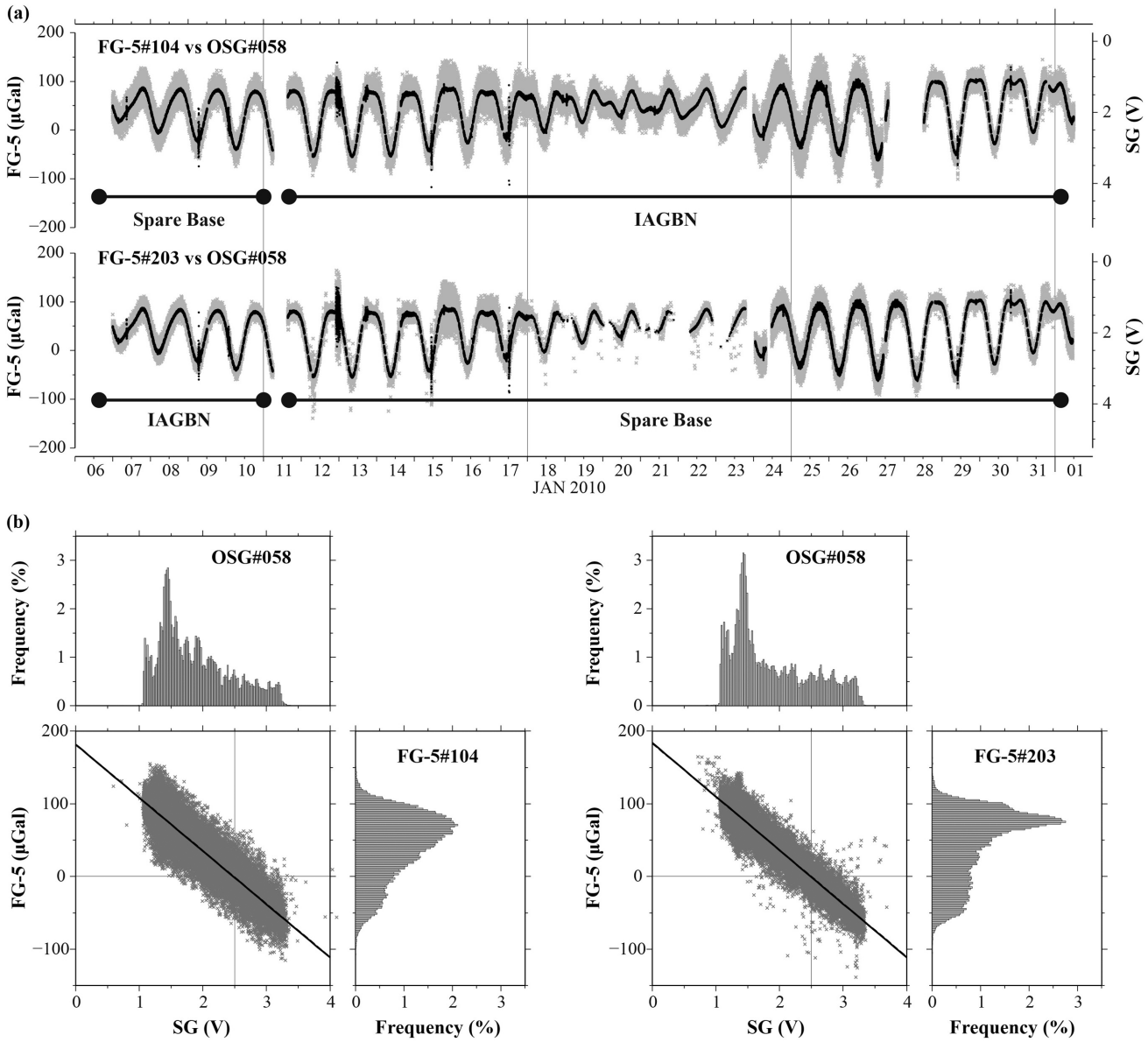

Figure 2. Comparison of FG5 and OSG#058. (a) Temporal variation between FG–5#104 and #203 (grey dots) and OSG#058 (black dots) and (b) their scatter diagrams and histograms for determining the scale factor. Histogram bin widths are 2 μGal for FG–5 and 0.02 V for OSG#058.

significant effect on the observed data. The previous two SGs required manual maintenance twice a year, during which wintering members were required to replenish the dewar with LHe. This operation significantly disturbed the gravity signal, and often induced step-like gravity changes. In comparison, OSG#058 showed no such disturbances in the gravity signal due to maintenance work. Indeed, the replenishment has not been made since February, 2010.

There were sharp changes in the temperatures of the first and second stages of the coldhead neck (downward spikes in Figs 3g and h) and in the pressure inside the dewar (upward spikes in Fig. 3l) in February, 2010, 2011, 2012, 2014, and January, 2012, 2013, 2014. These perturbations arose from the loss of cryocooler function caused by power failures at Syowa Station. However, in general, the power failures had no effect on the quality of the gravimetric signals (Fig. 3a).

Any rapid increase in atmospheric pressure (e.g. 2010 May 16 in Fig. 3k), as is typical after a blizzard, affected the pressure inside the dewar (downward spikes in Fig. 3(l). The heater power sometimes fluctuated (as shown by dots around 2.5 V in Fig. 3(j) to compensate the pressure inside the dewar, which in turn induced fluctuations in the tilt powers (Figs 3b and d) and tilt balances (Figs 3c and e). These fluctuations did influence the gravity signal at high-frequency bands from 5 to 50 s, but spectral analysis (Supporting Information Fig. S1) confirmed that a rapid increase in the atmospheric pressure did not affect the filtered and re-sampled data at 1 min intervals.

Fig. 4(a) shows the filtered gravity data at 1 min intervals for the 5 yr period of 2010 January 7–2015 January 10, together with the predicted tides computed using the tidal parameters obtained from 10 yr's observations with TT–70#016 (Iwano *et al.* 2005). The non-tidal gravity (grey line, Fig. 4b) is the difference between the observed and predicted tides. It varied within ± 20 μGal, except for the spike-like changes corresponding to significant earthquakes (e.g. Mw > 6). A beneficial feature of OSG#058 is that it does not require correction for step-like perturbations, so we can specify long-period gravity variations without estimating their spurious

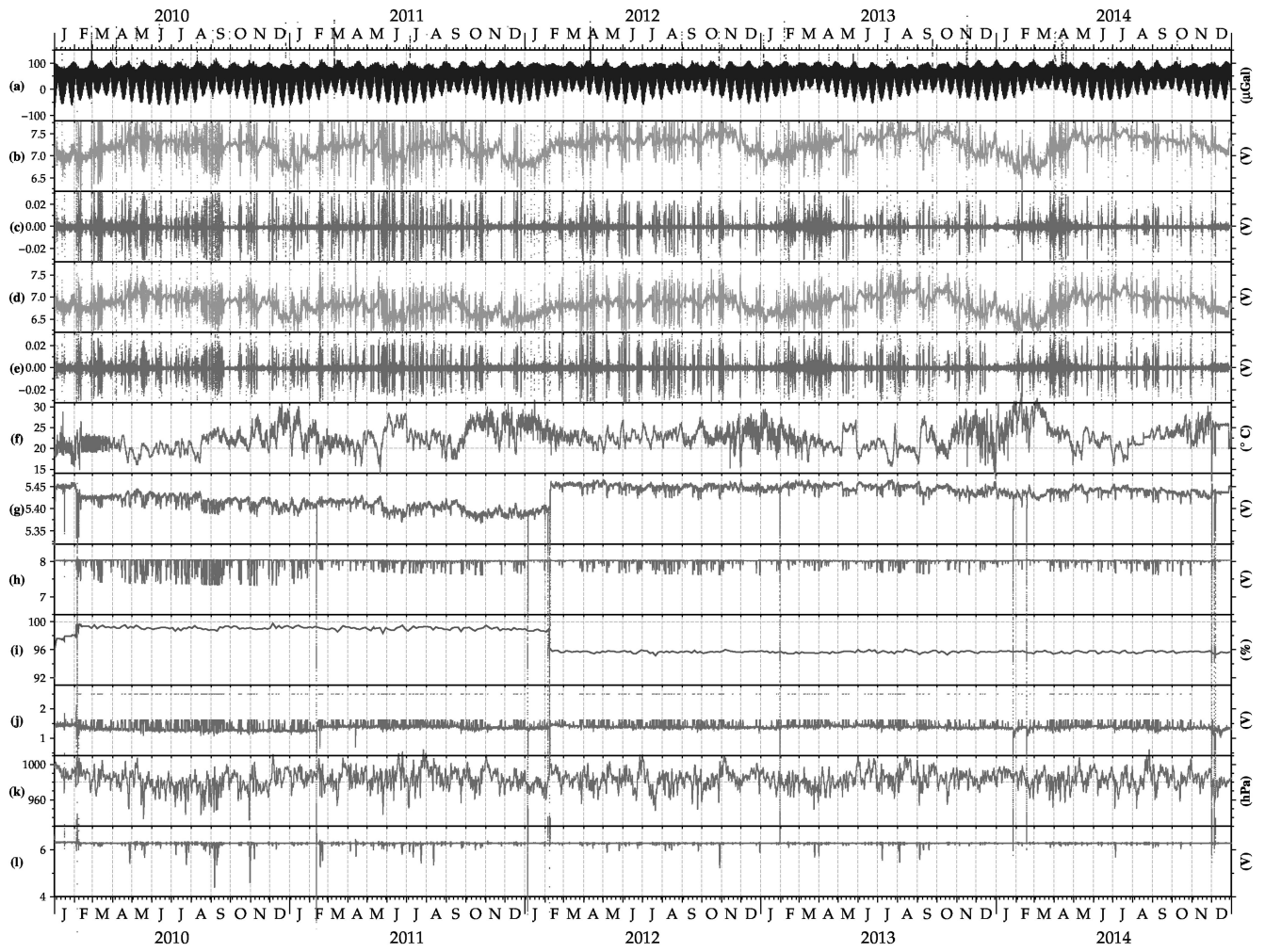

Figure 3. Yearly status plots of gravity and environmental data: (a) the gravity variations; (b) X tilt power; (c) X tilt balance; (d) Y tilt power; (e) Y tilt balance; (f) room temperature; (g) NKT1; (h) NKT2; (i) liquid helium level; (j) heater power in the dewar; (k) atmospheric pressure; (l) pressure inside dewar. NKT1 and NKT2 are inside temperatures at the first and second stages of the coldhead neck, respectively.

phases. Consequently, although the data period is limited to 5 yr, here we use only the high-quality OSG#058 data to deduce the long-term periodicity in the gravimetric variations.

2.4 Harmonic decomposition of tidal constituents and atmospheric effect

As in previous studies (Sato *et al.* 1995; Tamura *et al.* 1997; Iwano *et al.* 2005; Doi *et al.* 2008), we used a Bayesian tidal analysis program grouping method, BAYTAP–G (Tamura *et al.* 1991), for the harmonic decomposition of the short-period tidal constituents (called simply waves hereafter). Preprocessing involved re-sampling the 1 min interval filtered gravity and barometer data at 1 hr intervals. We applied BAYTAP–G to the 1 hr interval data to obtain the tidal parameters for the terdiurnal, semidiurnal and diurnal waves (short-period tides). BAYTAP–G can simultaneously deduce the atmospheric gravitational effects attributed to attraction and loading of atmospheric mass, by applying a barometric admittance method to the in-situ barometer data. Accordingly, BAYTAP–G decomposed the observed gravimetric time-series into four components: (1) short-period tidal waves, (2) atmospheric effects, (3) trend, and (4) short-term irregular noise. Note that this trend does not include short-period tidal waves, but does contain long-period tidal waves.

The trend time-series were passed through a digital low-pass filter with a cut-off period of 72 hr, and re-sampled to produce 1 d interval series, which were then decomposed by applying the BAYTAP–L program (a modified version of BAYTAP-G for long-period tidal analysis) into long-period tidal waves with periods from 4–5 d to semiannual waves.

2.5 Annual and 18.6 yr tides and polar motion effect

In addition to terdiurnal (M3) to semiannual (Ssa) waves, tidal gravity data are known to contain tidal waves with annual (Sa) and 18.6 yr (18.6yr) periods (combined as Sa+18.6yr) and the gravitational response to polar motion (i.e. the polar motion effect, PME). The Sa and 18.6yr tidal waves can be predicted from the Tamura's tidal potential (Tamura *et al.* 1987). For this we used tidal gravimetric factors of 1.159 and 1.161 without any phase lags for the Sa and 18.6yr waves, respectively, based on a latitude-dependent inelastic non-hydrostatic Earth model (Dehant *et al.* 1999).

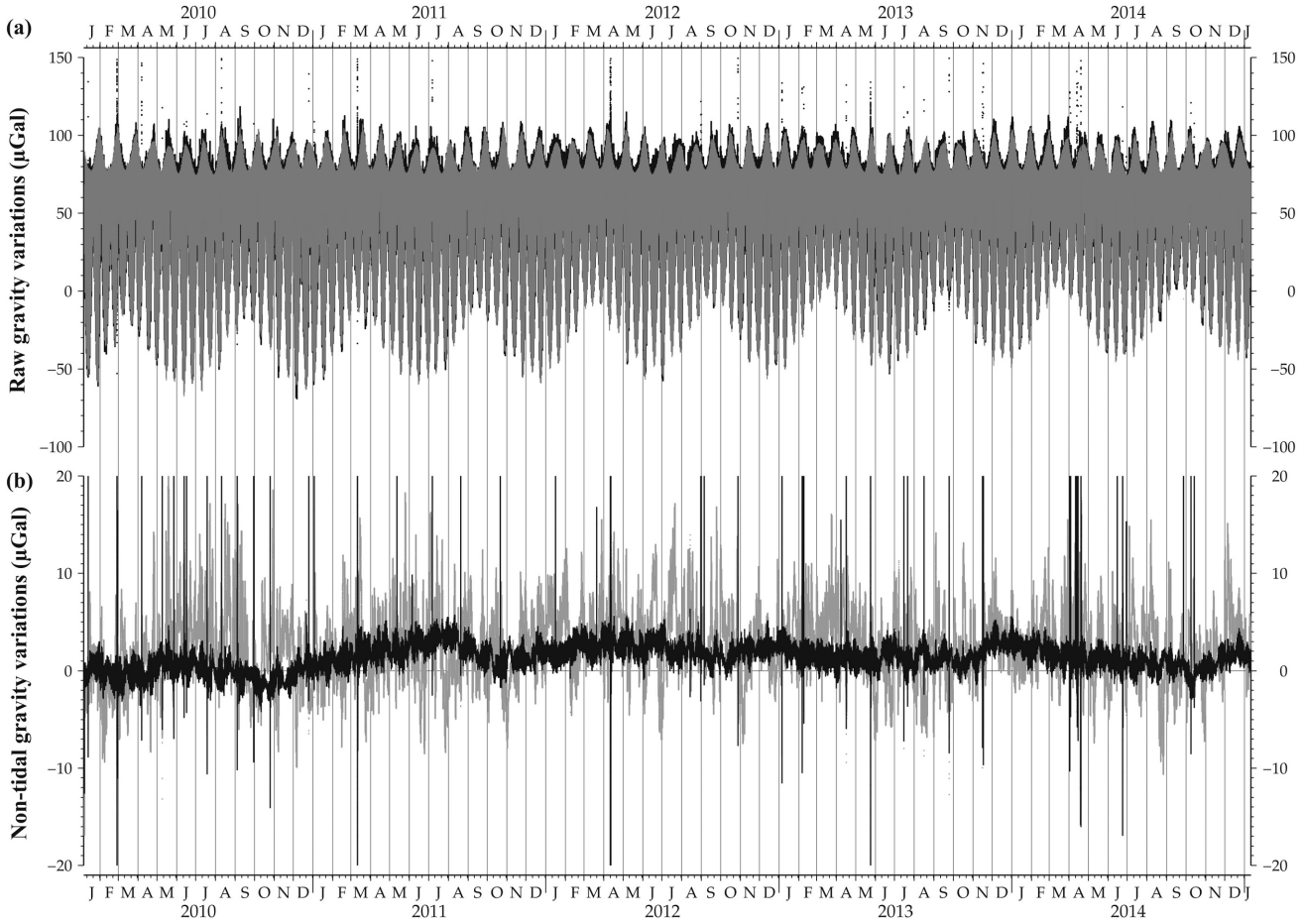

Figure 4. (a) 1 min interval gravity variations obtained with OSG#058 (black dots) and the predicted tidal components based on the tidal parameters of Iwano *et al.* (2005) (grey line). (b) Non-tidal gravity variations after subtraction of the predicted tidal components (grey line) and further subtraction of the atmospheric gravitational effects computed from *in-situ* barometer data by the admittance method (black line). The admittance coefficient used here is -0.360 μGal hPa^{-1}.

The variation in the centrifugal potential arising from perturbations in the Earth's rotation causes surface gravity variation, PME. The PME was estimated by eqs (3) and (4) of Wahr (1985), where we used the gravimetric factor of 1.159 (considering the Earth's elastic deformation). In this computation, the perturbations in the Earth's rotation were described by the Earth's orientation parameter (EOP) and eqs (3-18a) and (3-24a) of Eubanks (1993). The EOP values used here were EOP08C04 downloaded from the International Earth Rotation Service (http://www.iers.org/IERS/EN/DataProducts/EarthOrientationData/eop.html).

3 RESULT OF TIDAL ANALYSIS

3.1 Tidal waves

Fig. 5 shows (a) 1 hr interval data, (b) short-period and (c) long-period tidal waves decomposed with the BAYTAP–G and BAYTAP–L programs, (d) atmospheric effects, (e) short-term irregular noise, and (f) the residual of BAYTAP–L analysis. Note that there are no periods of missing observations and no step-like perturbations in the decomposed OSG#058 data.

The obtained tidal factor, phase, and amplitude of each wave (Table 1) agree well with those determined from the tidal analysis of 10 yr of TT–70#016 data (Iwano *et al.* 2005), despite the data period used here being half that by Iwano *et al.* (2005). Quantitatively, the maximum differences in the tidal factors are 0.45 per cent for the major diurnal and semi-diurnal waves (Q1, 01, M1, P1, K1, N2, M2, S2, K2) and 0.81 per cent for the major long-period waves (MTM, MF, MM); the maximum differences in the phases are 0.43 degree for the major diurnal and semi-diurnal waves and 0.64 for the major long-period waves. The root-mean-square errors (RMSEs) for the factor and the phase of each wave estimated here were 37 per cent and 38 per cent, respectively, larger than those estimated by Iwano *et al.* (2005). However, the RMSEs for MSTM, MTM, MSQM and MQM waves were 10 per cent better than their estimates.

The atmospheric effect estimated via barometric admittance resulted in a response coefficient of -0.360 ± 0.001 μGal hPa^{-1}. This value slightly differed from -0.375 ± 0.001 μGal hPa^{-1} by Iwano *et al.* (2005). This difference possibly arose from difference in the horizontal scale of the atmospheric pressure variation. According to fig. 3 of Boy *et al.* (2002), the response coefficients of -0.375 and -0.360 μGal hPa^{-1} represented the atmospheric pressure variations of the horizontal scale of about 1000 km and 1300 km, respectively.

Generally, there is a proportional relationship between spatial and temporal scales of the atmospheric pressure variation. Assuming that motions of the atmospheric mass are connected with the wind, the temporal scales are inferred by dividing the horizontal scale

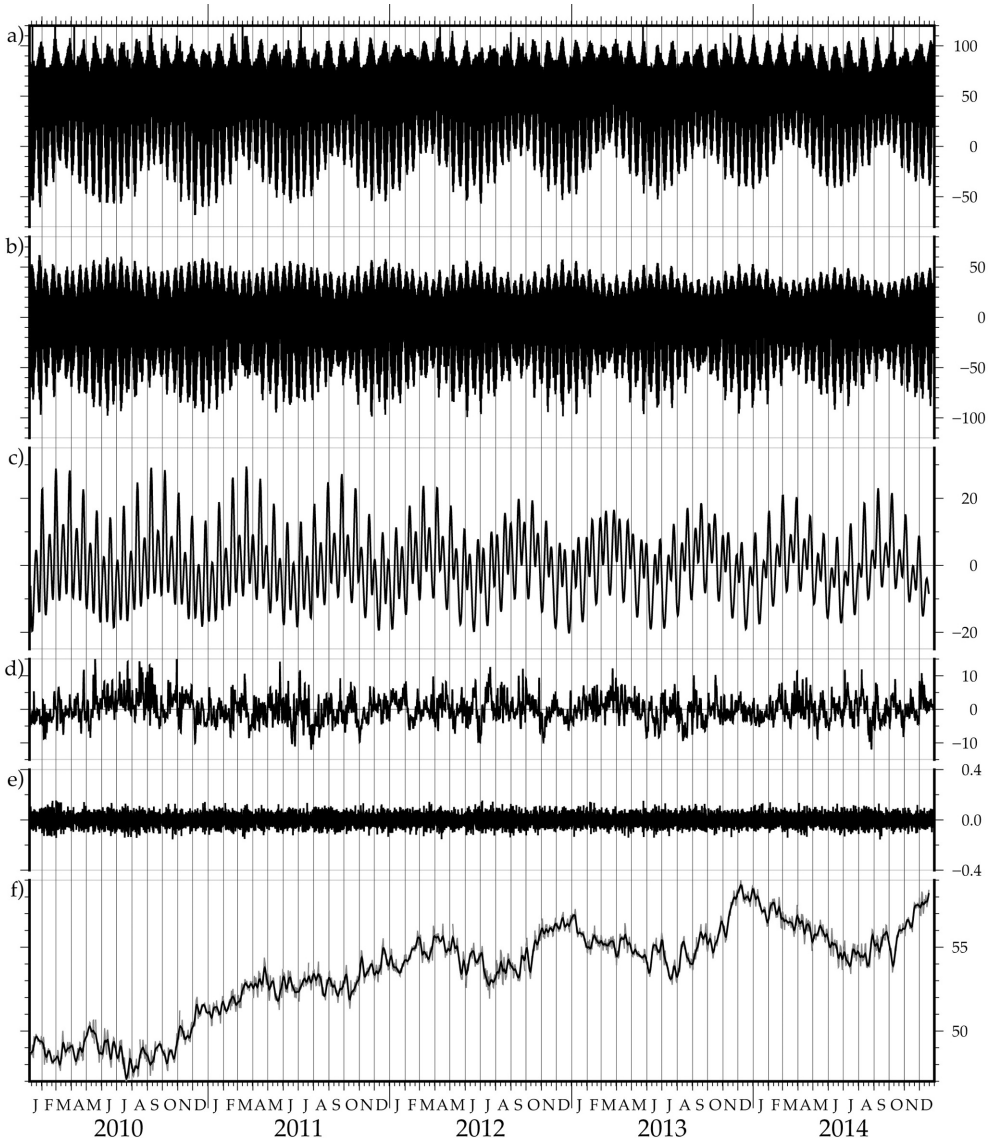

Figure 5. Result of tidal analysis. (a) 1 hr interval data obtained from OSG#058. (b) Short-period tidal waves. (c) Long-period tidal waves. (d) Atmospheric effects. (e) Short-term irregular noise. (f) The residual time-series of the BAYTAP–L analysis (the first non-tidal gravity variations). Unit of all vertical axes is μGal.

by the wind velocity. Both median values of hourly wind velocity data obtained at Syowa Station during 1997–2000 and 2010–2013 were 4.3 m s^{-1} (372 km d^{-1}). The inferred temporal scales for the horizontal scales of 1000 and 1300 km were 2.69 and 3.49 d, respectively. The spectral analysis of 4 yr's barometric data showed actual spectral peaks at 2.66 days (corresponding to 988 km) for the duration of 1997–2000, and at 3.41 d (corresponding to 1267 km) for the duration of 2010–2013. Moreover, the spectrum pattern (in the period of 2–4 d) of the duration of 2010–2013 agreed well with that of the duration of 1997–2000, which was shifted 0.8 d to a longer period in parallel with the frequency axis.

3.2 Non-tidal long-term gravity variations

The residuals of the BAYTAP–L analysis in Fig. 5(f) (termed here the first non-tidal gravity variations) contain long-term periodic variations with a peak-to-peak magnitude of ∼12 μGal. Fig. 6(a) shows that Sa+18.6yr waves dominated the long-term periodic variation of the first non-tidal residual gravity variations; the residuals after subtraction of these waves and a bias of 49.019 μGal, called the second non-tidal gravity variations, varied within a reduced range of about 7 μGal. It is clear from Fig. 6(b) that the PME approximates the long-period variation in the second non-tidal gravity variations. The residuals after subtraction of the PME (the third non-tidal gravity variations, solid curves in Fig. 6c) still retain seasonal and interannual variations with a linear increase ranging from −1.1 to 5.2 μGal.

4 SNOW EFFECTS ON GRAVITY VARIATIONS

In the Antarctic region, crustal uplift due to GIA is usually recognizable as a time-dependent decrease in the local gravitational field. However, the third non-tidal gravity variations exhibit an increasing trend of about 1.2 μGal for the 5 yr observation period, which corresponds to a crustal subsidence. Moreover, the third non-tidal

Table 1. Observed tidal parameters without ocean tide correction.

Wave	Tidal factor (RMSE)	Phase (RMSE) [deg]	Amp. (RMSE) [μGal]
Ssa	1.0694 (0.2943)	−0.30 (15.78)	5.164 (1.421)
Msm	1.0879 (0.0834)	−0.70 (4.41)	1.141 (0.087)
Mm	1.1206 (0.0118)	0.32 (0.60)	6.144 (0.065)
Msf	1.1220 (0.0253)	−2.53 (1.29)	1.020 (0.023)
Mf	1.1284 (0.0023)	−0.75 (0.12)	11.710 (0.024)
Mstm	1.2532 (0.0363)	−5.05 (1.67)	0.473 (0.014)
Mtm	1.1365 (0.0075)	−0.15 (0.38)	2.258 (0.015)
Msqm	0.9965 (0.0407)	−0.89 (2.35)	0.316 (0.013)
Mqm	1.0150 (0.0479)	−5.96 (2.71)	0.267 (0.013)
4–5 days	1.0785 (0.1315)	3.93 (7.02)	0.083 (0.010)
Q1	1.30265 (0.00156)	−2.273 (0.069)	5.189 (0.006)
O1	1.27465 (0.00029)	−0.763 (0.013)	26.519 (0.006)
M1	1.24686 (0.00316)	−0.225 (0.145)	2.040 (0.005)
$\pi 1$	1.22763 (0.00855)	0.581 (0.399)	0.695 (0.005)
P1	1.22049 (0.00051)	−0.191 (0.024)	11.815 (0.005)
S1	1.19215 (0.02318)	−5.603 (1.114)	0.273 (0.005)
K1	1.20522 (0.00017)	−0.191 (0.008)	35.264 (0.005)
$\Psi 1$	1.27097 (0.01827)	0.327 (0.824)	0.291 (0.004)
$\phi 1$	1.22437 (0.01100)	−0.436 (0.515)	0.510 (0.005)
J1	1.20476 (0.00271)	−0.786 (0.129)	1.971 (0.004)
OO1	1.20911 (0.00499)	−1.816 (0.236)	1.082 (0.004)
2N2	1.31139 (0.00352)	−5.923 (0.154)	0.321 (0.001)
N2	1.43357 (0.00071)	−1.202 (0.029)	2.650 (0.001)
M2	1.40508 (0.00014)	−0.768 (0.006)	13.565 (0.001)
$\lambda 2$	1.41801 (0.01641)	−1.783 (0.663)	0.101 (0.001)
L2	1.44829 (0.00587)	−1.356 (0.232)	0.395 (0.002)
T2	1.51529 (0.00491)	−1.818 (0.186)	0.398 (0.001)
S2	1.50356 (0.00029)	1.082 (0.011)	6.753 (0.001)
K2	1.51942 (0.00117)	0.499 (0.044)	1.855 (0.001)
M3	1.09132 (0.00957)	19.380 (0.502)	0.074 (0.001)

Note that phase lags are positive values.

gravity variations also show seasonal and interannual periodic variations. These features indicate that the GIA response is obscured by other variations in the Earth's surface mass by, for example, the atmosphere, ocean, and snow.

In this section, we infer influences of these variations on the third non-tidal gravity variations from the previous studies (in Section 4.1). Especially, we focus the gravitational effect of the heavy snowfall (the snow accumulation) in DML (Boening *et al.* 2012; Shepherd *et al.* 2012) to the OSG#058 observation (in Section 4.2). The estimation of this gravitational effect is verified by considering a simple attractive force model (in Section 4.3) and by comparing with the GRACE data (in Section 4.4).

4.1 Gravitational effects of Earth's surface mass variations

We estimated empirically (by admittance) the atmospheric gravitational effects from the simultaneous local barometric data. However, the empirical results and those from sophisticated methods using the gridded atmospheric elements from the global numerical weather forecasts differed by less than 1 μGal for periods of more than 100 d (Boy *et al.* 2002). This result cannot account for the decade-time-scale gravity increase observed at Syowa Station (Fig. 6c).

Previous estimations of the gravitational effect due to the non-tidal mass redistribution in the ocean at Syowa Station, using sea surface heights of the global ocean general circulation model and Topex/Poseidon altimetry data (Sato *et al.* 2001), found that annual variation was a dominant component; however, the magnitude of the annual variation was less than 1 μGal. Rye *et al.* (2014) exhibited the linearly rise of the sea surface height around the Antarctica attributed to the increased glacial discharge. On the other hand, the amplitude of periodic component seemed not to vary for two decades according to their fig. 2. We then considered that the oceanic gravitational effect was not a major source for the seasonal and interannual variations in the third non-tidal gravity variations exceeding 5 μGal in Fig. 6(c), although there was possibility that it obscures the GIA response.

In the case of SGs in Europe, the hydrological gravitational effects due to groundwater and soil moisture dominated the non-tidal long-term gravity variations (e.g. Crossley *et al.* 2012). On the other hand, there is no sedimentary layer around Syowa Station and the temperature is below the freezing point all year around, so that neither groundwater nor soil moisture effect is detected at Syowa Station. Such hydrological gravitational effects cannot be sources of the third non-tidal gravity variations.

The satellite GRACE data indicate an increase of the surface mass in East Antarctica, especially in the coastal region of DML after 2009 (e.g. Boening *et al.* 2012; Shepherd *et al.* 2012). This was attributed presumably to increased snowfall in this region (Boening *et al.* 2012; Lenaerts *et al.* 2013). We examine whether this increase in snowfall can account for the observed decade-time-scale increase in the third non-tidal gravity variations seen in Fig. 6(c).

4.2 Snow accumulation

Syowa Station is located in the coastal region of DML. Heavy snowfall since 2009 has made the icebreaker's access difficult, and snow

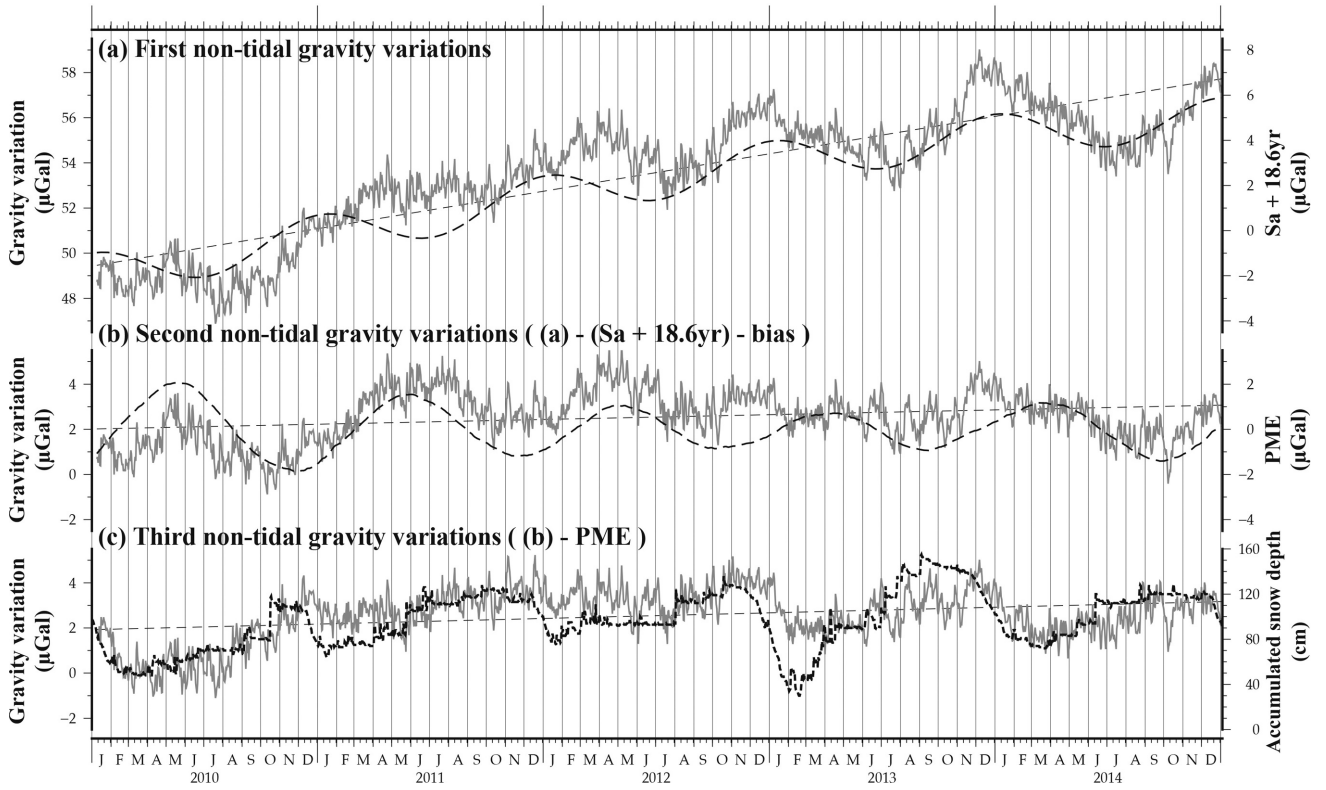

Figure 6. Non-tidal gravity variations (grey solid line) compared with the following components (black dotted curves): (a) the annual and 18.6 yr tidal waves (Sa+18.6yr), (b) polar motion effect, and (c) the accumulated snow depth. Grey dotted straight line in each panel depicts the linear trend listed in Table 2.

accumulation has also increased since then. Daily data sets of the accumulated snow depth have been measured at a site (39.58575°E, 69.00481°S) in Syowa Station (see Fig. 1c for the site location) by wintering members from the Japan Meteorological Agency (the data sets are available from http://www.jma.go.jp/jma/index.html).

Fig. 6(c) shows good agreement between the third non-tidal gravity variations and the accumulated snow depth. The significance of the cross-correlation exceeds the 99 per cent confidence level based on the t-distribution test (Fig. 7a). The maximum correlation appeared at a lag of 21 d for the third non-tidal gravity variations against the accumulated snow depth, indicating snow as the cause of the variations. A blizzard could cause a sudden increase of 20–40 cm in the accumulated snow depth. The new snow could compact the previous snow layer, gradually increasing its density while decreasing its thickness and porosity. Given that the SG is sensitive only to the vertical attraction of the snow mass, it is affected only by the snow mass below the height of its gravity sensor and not by any snow mass surrounding it laterally. Snow compaction lowers the position of the centre of snow mass, and thus gradually increases the vertical attraction. The delay of 21 d probably represents the delay in snow compaction (densification).

The accumulated snow depth (with a delay of 21 d) on the x-axis of the scatter diagram in Fig. 7(b) shows a linear relationship with the third non-tidal gravity variations on the y-axis. The gravitational effect of the accumulated snow mass (hereinafter referred to as the accumulated snow mass effect, ASME) can be computed from the following liner relationship,

$$\mathrm{ASME}(t) = a_c \times S_d(t - L) + b, \quad (1)$$

where t is time variable, a_c is a conversion factor, S_d is the accumulated snow depth, L is the time lag (here 21 d for the maximum correlation), and b is constant bias. This equation gives values of 3.13 ± 0.08 μGal m^{-1} for a_c and -0.45 ± 0.08 μGal for b.

Fig. 7(c) shows the third non-tidal gravity variations (light grey line), ASME (blue line) and their difference (red line). The ASME varied within a range of 0.6–4.9 μGal, with an average of 3.01 μGal. After subtraction of this ASME, the resultant final non-tidal gravity variations (red line in Fig. 7c) showed a peak-to-peak magnitude of 5.2 μGal, with an average of −0.47 μGal. In addition, the final non-tidal gravity variations had a 0.31 μGal smaller standard deviation than the third non-tidal gravity variations.

A frequency histogram for the third non-tidal gravity variations (shaded area in Fig. 8) represents a left-skewed asymmetric distribution with a skewness of −0.67. The skewness of the frequency distribution for the final non-tidal gravity variations was −0.23, with an approximately symmetric shape. This confirms that the left-skewed asymmetric distribution of the third non-tidal gravity variations can be attributed to the ASME.

The slope of the straight line fitted to the third non-tidal gravity variations was 0.25 ± 0.02 μGal yr^{-1} (Table 2), which corresponded to the crustal subsidence, not uplift, rate of 1.0 mm yr^{-1} based on the ratio between the gravity variation and the vertical displacement of −0.26 μGal mm^{-1} (de Linage *et al.* 2007). On the other hand, the slope for the final non-tidal gravity variations was 0.08 ± 0.02 μGal/year. The linear increase in the final observed non-tidal gravity reduced to one third of its magnitude after subtraction of the ASME. Given that the crustal deformation in a vertical direction is almost zero (less than 0.4 mm yr^{-1}) according to the GNSS and DORIS measurements (http://apps.ids-doris.org/apps/stcdtool.html) at Syowa Station in the last decade, OSG#058 has surely detected the gravity variations associated with ASME.

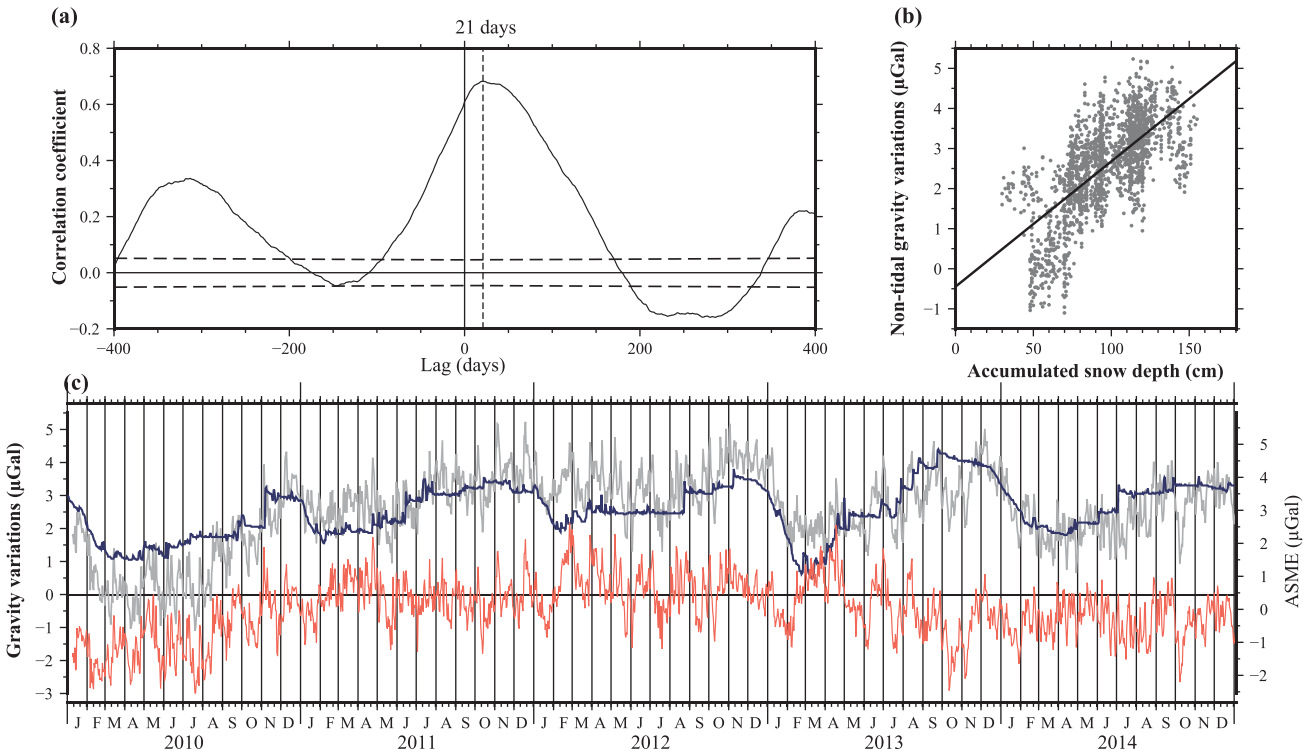

Figure 7. (a) Cross correlation between the accumulated snow depth and the third non-tidal gravity variations. (b) Their scatter diagram. (c) Comparison of the third non-tidal gravity variations (light grey line) with the accumulated snow mass effect (blue line) and their residual (red line).

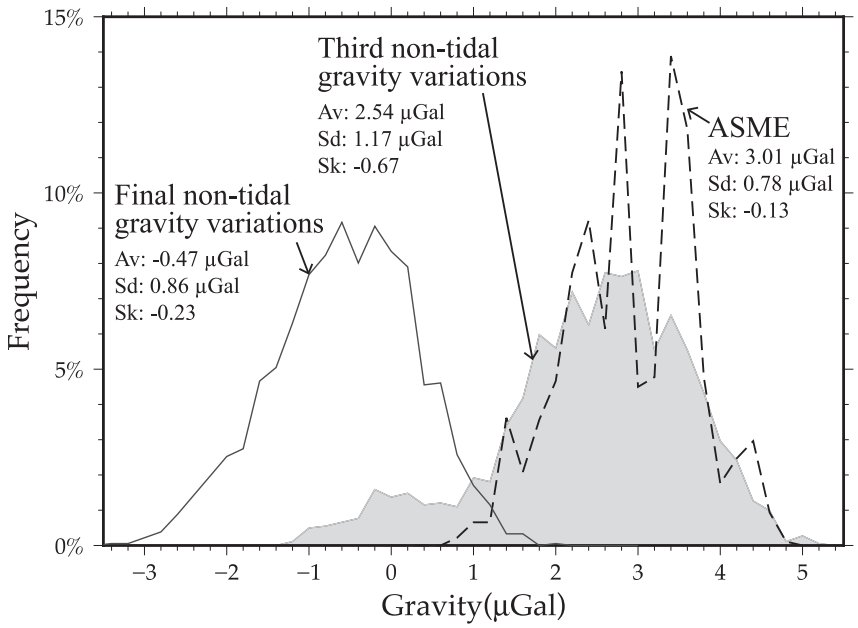

Figure 8. Histograms of the third non-tidal gravity variations, the accumulated snow mass effect, and the final non-tidal gravity variations. Bin width of all histograms is 0.5 μGal.

4.3 Estimation of accumulated snow density

We examined whether the estimated conversion factor, a_c in eq. (1), was realistic. The measurement site for accumulated snow depth was located 250 m from the GOH. Given that the GOH (8 × 6 × 3 m) was built directly on the bedrock and there was no groundwater, we roughly considered the attractive force due to a hollow-cylinder-shaped accumulated snow mass as illustrated in Fig. 9. The attractive force of the hollow-cylinder-shaped mass, A_{hc} (μGal), can be expressed as

$$A_{\mathrm{hc}} = 2\pi G\rho \times\left[\sqrt{r_a^2+(z-h)^2}-\sqrt{r_a^2+z^2}-\sqrt{r_b^2+(z-h)^2}+\sqrt{r_b^2+z^2}\right]\times 10^8, \quad (2)$$

Table 2. Estimated linear trend (slope) by linear regression.

	Linear trend [μGal yr^{-1}]
First non-tidal gravity variations	1.658 ± 0.015
Second non-tidal gravity variations	0.212 ± 0.015
Third non-tidal gravity variations	0.248 ± 0.015
Final non-tidal gravity variations	0.077 ± 0.015
ASME	0.183 ± 0.007

where G is the gravitational constant, ρ is density of mass, r_a and r_b are outside and inside radii of the hollow-cylinder-shaped mass, h is its height and z is a height of the sensing unit of OSG#058 from the base of hollow-cylinder-shaped mass (see Fig. 9). An averaged ellipsoidal height within 250 m of radius from GOH was computed from the GSI digital elevation model (http://antarctic.gsi.go.jp/seika-e.html); its relative height to the sensing unit of OSG#058 is −1.7 m, so we use $z = 1.7$ m. In a case that $r_a = 250$ m and $r_b = 4\sqrt{2}$ m are used, the a_c factor means that such hollow-cylinder-shaped snow with 1 m thickness exerts a downward attraction of 3.13 μGal on the OSG#058. In this case, the density of snow (ρ in eq. 2) can be calculated as 372.3 kg m^{-3}.

The density of dry and tightly compacted snow usually ranges from 300 to 550 kg m^{-3}, and the near-surface snow density on the Antarctic ice sheet about 200 km away from Syowa Station was found to be about 400 kg m^{-3} (e.g. Sugiyama *et al.* 2012). This suggests that our estimate of a_c is not unrealistic. In future, we plan to measure the distribution of accumulated snow and then make a digital elevation model of the accumulated snow to evaluate the loading effect as well as the attractive force, in order to separate the ASME from the long-term non-tidal gravity variations.

4.4 Comparison with satellite gravity data

OSG#058 detected the ASME caused by the snow mass around the GOH. Next, we examined whether the accumulated snow depth at Syowa Station correctly reflected extensive surface mass changes in DML. For this purpose, GRCTellus Land data (Landerer & Swenson 2012; Swenson 2012), which provided terrestrial water storage data estimated from the spherical harmonic coefficients of GRACE, were used as the surface mass change data. Unscaled values of the liquid water equivalent (LWE) thickness at three points around Syowa Station, (39.5°E, 69.5°S), (40.5°E, 69.5°S) and (39.5°E, 70.5°S), were extracted from the above GRCTellus Land data at approximately one month intervals. Temporal variations of these LWEs were compared with the long-period temporal variations of the accumulated snow depth data, which were smoothed with a 120 d Gaussian filter, as shown in Fig. 10(a). This comparison demonstrates the good agreements in the trends between LWEs and the accumulated snow depth at Syowa station, although the latter has large seasonal variations that are not seen in the former.

The greatest cross-correlation (0.747) between the LWE at (39.5°E, 69.5°S) and the accumulated snow depth appears at zero lag; this value exceeds the 99 per cent confidence level. Applying a simple linear regression to both data gives 0.264 ± 0.02 cm-H_2O/cm (=264 ± 2 kg m^{-3}) for the slope as shown in the right panel of Fig. 10(a); this value was 34 per cent smaller than the approximated snow density of 400 kg m^{-3} in this area. The LWE signals of the GRCTellus Land data are typically attenuated by truncation of spherical harmonic coefficients and the application of two filters (the de-striping filter and the Gaussian smoothing filter with a 300 km radius), so that scaling is necessary for accurate estimates (Landerer & Swenson 2012). Velicogna & Wahr (2013) presented various errors influencing estimates of the GRACE-derived ice sheet mass change, and evaluated 38–48 per cent signal reduction in the Antarctic ice sheet due to both truncation and filtering. Assuming that the LWE signals are not attenuated, the snow density estimated from the slope of the simple linear regression becomes 264 kg m^{-3}/(1 − 0.48) = 508 kg m^{-3}. Although there remained uncertainty in the magnitude, it was plausible that the accumulated snow depth at Syowa Station is representative of the surface mass change of a wide area corresponding to the 300 km radius.

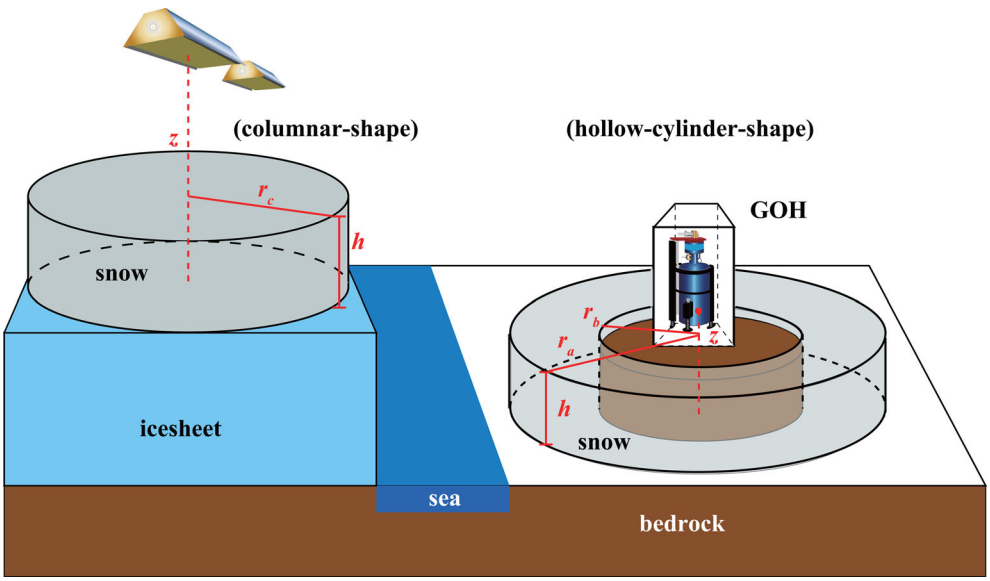

Figure 9. Schematic diagram of positional relations between the accumulated snow mass, OSG#058 and GRACE for estimating attractive forces of the accumulated snow mass. Since GOH is built directly on the bedrock, the accumulated snow is distributed approximately with a hollow-cylinder-shape. It is noted that there is no sedimentary layer in Syowa Station and therefore neither groundwater nor soil moisture effect which obscures interpretation of gravitational effects.

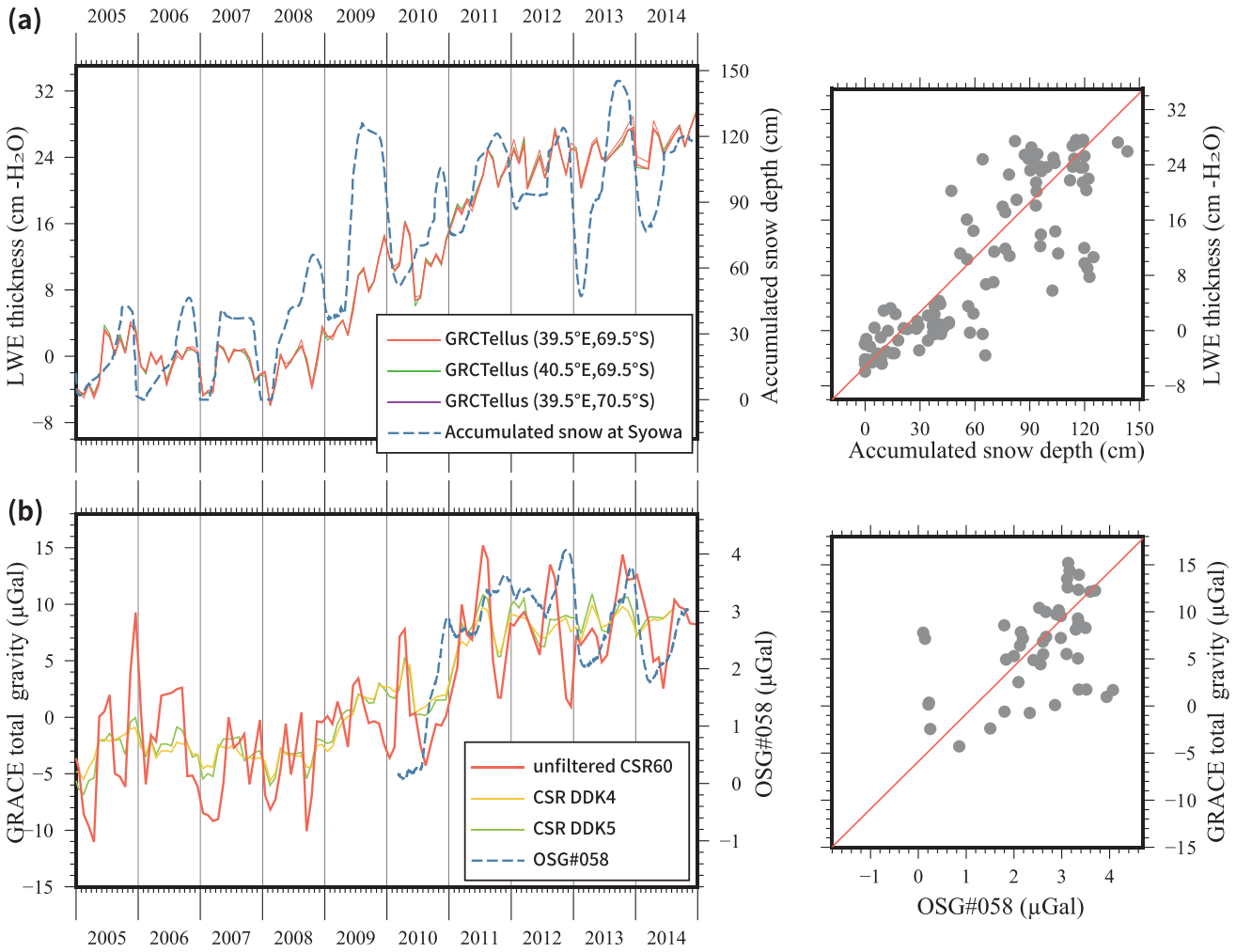

Figure 10. Comparisons of ground and satellite gravity data. (a) Comparison of the accumulated snow depth at Syowa Station with the liquid water equivalence (LWE) thickness in GRCTellus. (b) Comparison of the third non-tidal gravity variations obtained from OSG#058 with GRACE-derived total gravity variations. The left columns exhibit comparisons in time-series. The right columns show the scatter diagrams between LWE at (39.5°E, 69.5°S) and the accumulated snow depth (a), and between the unfiltered GRACE-derived total gravity variations (unfiltered CSR60) and OSG#058 (b).

Syowa Station is located on a small island (East Ongul Island) 3 km from the Antarctic ice sheet, as shown in Fig. 1(c). An extensive surface mass change on the ice sheet may affect the gravity observations by OSG#058 through attractive force and loading effect; these gravitational effects can be computed by applying the method of Doi *et al.* (2010), which used Farrell Green's function (Farrell 1972) and empirical snow density model. The estimated attractive force and loading effect induced by a 1 m increase of accumulated snow depth on area A in Fig. 1(b) were −0.0678 and 0.0479 μGal, respectively, while those on area B were 0.0014 and 0.0157 μGal, respectively. The average heights above sea level of the areas A and B were about 450 and 910 m, respectively, while their (elevation, azimuth, distance) from OSG#058 were (+1.3°, N88°E, 17 km) and (−0.3°, N178°E, 139 km), respectively.

Snow masses at the two areas, which were mainly distributed laterally relative to OSG#058, hardly induced a vertical component of attraction force. The total gravity changes were −0.02 μGal for area A and 0.02 μGal for area B. These values were smaller in magnitude compared with the ASME in the vicinity of OSG#058, and cancelled each other out. The areas A and B located near the three grid points (39.5°E, 69.5°S), (40.5°E, 69.5°S) and (39.5°E, 70.5°S) of the GRCTellus Land data plotted in Fig. 10(a). Accordingly, even if there were extensive surface mass changes on the Antarctic ice sheet, consistent with the accumulated snow depth at Syowa Station, they would not affect the OSG#058 gravity observations. To use only the depth (or mass) of accumulated snow observable at Syowa Station was reasonable in the estimation of the ASME affecting the OSG#058 observations.

Finally, we compared the third non-tidal gravity variations obtained from OSG#058 with GRACE satellite gravity data directly (Fig. 10b). The time-series of total gravity variations above Syowa Station were computed from monthly data sets of spherical harmonic coefficients of the GRACE gravity field provided by Center for Space Research at University of Texas, Austin (CSR, Level 2 solution, release 05) from January 2005 to January 2015. We used SHTOOLS (http://shtools.ipgp.fr) to convert the spherical harmonic coefficients into gravity variations with truncation at 60 degrees and without the spatial filtering. To compare them at longer periods, the Gaussian filter of 120 d was adapted for both time-series of the SG third non-tidal gravity variations and the GRACE total

gravity variations. To examine striping effects, we also considered the GRACE total gravity variations computed from monthly data sets of the non-isotropic filtered spherical harmonic coefficients (DDK4 and 5 by Kusche 2007). The filtered and unfiltered satellite gravity variations were consistent. Therefore, unfiltered satellite gravity variations can be used in comparisons with the SG ground gravity variations.

As shown in Fig. 10(b), both satellite and ground gravity variations showed increases after 2010, with good agreement in their trends. The cross-correlation between the two gravity variations was 0.456 (at zero lag), and was greatest (0.615) with a 2 month lag of the ground data, where both values exceeded the 99 per cent confidence level. Their linear relationship (right panel in Fig. 10b) shows that the satellite gravity variations were 5.1 ± 0.6 times larger than the ground ones.

Comparison of the ground gravity variations obtained from several SGs in Europe with the GRACE-derived gravity variations shows good agreements in both magnitude and trend for extensive (global) gravity variations (e.g. Neumeyer *et al.* 2008; Weise *et al.* 2009; Crossley *et al.* 2012). Crossley *et al.* (2012) also demonstrated good agreement between SG and GRACE-derived gravity variations through a single station comparison without excluding local hydrological gravitational effects.

Our results differ from those of the studies mentioned above. The OSG#058 gravity variations were considerably smaller than those derived from GRACE; this was probably due to the vertical distribution of the mass attracting on the SG and GRACE satellites. In the case of the SGs over Europe, the primary attraction sources near them were groundwater and soil moisture, which were located below both the SGs and GRACE. In contrast, the accumulated snow mass on the Antarctic ice sheet was distributed lateral to or above the SG and below the GRACE satellites (Fig. 9). As the OSG#058 was installed directly on the bedrock, as described in Section 4.3, the attractive force of accumulated snow affecting it can be estimated as 3.36 μGal from eq. (2) by assuming the hollow-cylinder-shaped snow mass with $h = 1$ m, $r_a = 250$ m, $r_b = 4\sqrt{2}$ m, $\rho = 400$ kg m^{-3}, and $z = 1.7$ m. On the other hand, the attractive force affecting the GRACE-derived gravity can be estimated by assuming a columnar-shaped snow mass:

$$A_{\rm col} = 2\pi G\rho \left[h + \sqrt{r_c^2 + (z-h)^2} - \sqrt{r_c^2 + z^2} \right] \times 10^8, \qquad (3)$$

where r_c and h are radius and height of the columnar-shaped snow mass, z is an altitude of GRACE (Fig. 9). Given that $r_c = 300$ km, $h = 1$ m, $\rho = 508$ kg m^{-3}, and $z = 400$ km, the estimated $A_{\rm col}$ was 4.26 μGal; this value was 1.3 times of $A_{\rm hc}$ affecting the ground SG. Although the unfiltered GRACE-derived gravity variations were also 27 per cent attenuated by the truncation (Velicogna & Wahr 2013), these simple attractive force models with different snow mass distribution relative to each sensor were incapable of accounting for the 5.1 times larger magnitude of the GRACE-derived gravity variations than the ground gravity variations observed by OSG#058. This implied that the accumulated snow mass detected by GRACE could not entirely affect the OSG#058 gravity observations. As mentioned above, the OSG#058 was insensitive to the attractive force of the accumulated snow mass on the area B because the elevation angle of the area B from the GOH was almost 0° (Supporting Information Fig. S2). If the accumulated snow mass detected by GRACE were densely and inhomogeneously distributed in such area (yellow-coloured area in Supporting Information Fig. S2b), OSG#058 would not detect their attractive forces. On the contrary, the detailed comparison between the GRACE-derived and the ground OSG#058 gravity variations may be useful for revealing in inhomogeneous distribution of the accumulated snow mass in DML.

5 CONCLUSIONS

Continuous gravity observations have been performed over 20 yr with three successive generations of SG (TT–70#016, CT#043, and OSG#058) at Syowa Station, East Antarctica. The third-generation SG, OSG#058, has recorded high-quality data since 2010 January 6 without missing observations or detectable drifts. Its 5 yr of data have never been disturbed by any step-like changes, and are used here to examine long-periodic gravity variations.

To extract the long-period non-tidal gravity variations, the 5 yr's data from January 2010 to January 2015 were decomposed into tidal waves (M3 to Ssa) and other long-period components. The non-tidal gravity variations, which were obtained by subtracting Sa and 18.6yr tidal waves and the predicted PME from the above long-period residuals, exhibited seasonal and interannual periodic variations with a linear increase ranging from −1.1 to 5.2 μGal.

The resultant long-period gravity variations significantly correlated with accumulated snow depths measured at Syowa Station. Their maximum correlation appeared at a lag of 21 d for the gravity variations against the accumulated snow depth. To estimate the ASME on gravity, we deduced a conversion factor of 3.13 ± 0.08 μGal m^{-1}. The estimated ASME varied within the range of 0.6–4.9 μGal. Subtracting the ASME from the long-period gravity residuals removed the left-skewed asymmetric frequency distribution shown in the above residuals.

The snow accumulation at Syowa Station, which was detected by the OSG#058, agreed well with terrestrial water storage estimated from the GRACE data around Syowa Station. This feature suggested that the snow accumulation at Syowa Station represented the surface mass balance (the snow accumulation) in a broad region (on the ice sheet around Syowa Station) in DML, which was detected by the GRACE satellite gravity observation. These results suggested a possibility of the ground gravity observation at Syowa Station to estimate the snow accumulation on the ice sheet around Syowa Station in DML.

ACKNOWLEDGEMENTS

This research was part of the Science Program of the Japanese Antarctic Research Expedition (JARE), supported by the National Institute of Polar Research (NIPR) under the Ministry of Education, Culture, Sports, Science and Technology (MEXT). Continuous SG observations were conducted by the 34th to the 55th Expeditions. GRCTellus data used in this study were downloaded from http://grace.jpl.nasa.gov, supported by the NASA MEaSUREs Program. GSI digital elevation model in Prince Olav Coast and Souya Coast Area was produced in 2010 as Technical material No. C1-406. The publication of this paper was supported by an NIPR publication subsidy. The authors are grateful to Yoichi Fukuda and another anonymous reviewer for their helpful and insightful comments.

REFERENCES

Aoyama, Y., Ikeda, H., Hayakawa, H., Doi, K., Fukuda, Y. & Shibuya, K., 2015. Observation and data archiving system of a superconducting gravimeter at Syowa Station, Antarctica, *Int. J. Geosci.,* **6,** 1116–1126.

Boening, C., Lebsock, M., Landerer, F. & Stephens, G., 2012. Snowfall-driven mass change on the East Antarctic ice sheet, *Geophys. Res. Lett.,* **39,** L21501, doi:10.1029/2012GL053316.

Boy, J.-P., Gegout, P. & Hinderer, J., 2002. Reduction of surface gravity data from global atmospheric pressure loading, *Geophys. J. Int.,* **149**(2), 534–545.

Chen, J.L., Wilson, C.R. & Tapley, B.D., 2006. Satellite gravity measurements confirm accelerated melting of Greenland ice sheet, *Science,* **313,** 1958–1960.

Chen, J.L., Wilson, C.R., Blankenship, D. & Tapley, B.D., 2009. Accelerated Antarctic ice loss from satellite gravity measurements, *Nat. Geosci.,* **2,** 859–862.

Crossley, D., Linage, C., Hinderer, J., Boy, J.-P. & Famiglietti, J., 2012. A comparison of the gravity field over Central Europe from superconducting gravimeters, GRACE and global hydrological models, using EOF analysis, *Geophys. J. Int.,* **189**(2), 877–897.

Dehant, V., Defraigne, P. & Wahr, J., 1999. Tides for a convective Earth, *J. geophys. Res.,* **104**(B1), 1035–1058.

de Linage, C., Hinderer, J. & Rogister, Y., 2007. A search for the ratio between gravity variation and vertical displacement due to a surface load*Geophys. J. Int.,* **171**(3), 986–994.

Doi, K., Shibuya, K., Ikeda, H. & Fukuda, Y., 2008. Continuous gravity observation with the superconducting gravimeter CT #043 at Syowa Station, Antarctica, in *Geodetic and Geophysical Observations in Antarctica,* pp. 237–247, eds Capra, A. & Dietrich, R., Springer-Verlag.

Doi, K., Shibuya, K., Aoyama, Y., Ikeda, H. & Fukuda, Y., 2010. Observed gravity change at Syowa Station induced by Antarctic ice sheet mass change, *IAG Symposia,* **135,** Springer, 557–562, doi:10.1007/978-3-642-10634-7_74.

Eubanks, T.M., 1993. Variations in the orientation of the Earth, in *Contributions of Space Geodesy to Geodynamics, Geodyn. Ser.,* Vol. 24, pp. 1–54, eds Smith, D.E. & Turcotte, D.L., AGU.

Farrell, W.E., 1972. Deformation of the Earth by surface loads, *Rev. Gerphys. Space Phys.,* **10,** 761–797.

Ikeda, H., Doi, K., Fukuda, Y., Tamura, Y. & Shibuya, K., 2005. Installation of the superconducting gravimeter CT(#043) at Syowa Station, Antarctica, *Polar Geosci.,* **18,** 49–57.

Ikeda, H., Aoyama, Y., Hayakawa, H., Doi, K. & Shibuya, K., 2011. Development of the superconducting gravimeter using a new type of diaphragm, *Physica C,* **471,** 1543–1546.

Iwano, S., Kimura, I. & Fukuda, Y., 2003. Calibration of the superconducting gravimeter TT70#016 at Syowa Staion by parallel observation with the absolute gravimeter FG5#203, *Polar Geosci.,* **16,** 22–28.

Iwano, S., Fukuda, Y., Sato, T., Tamura, Y., Matsumoto, K. & Shibuya, K., 2005. Long-period tidal factors at Antarctica Syowa Station determined from 10 years of superconducting gravimeter data, *J. geophys. Res.,* **110,** B10403, doi:10.1029/2004JB003551.

Kim, T.-H., Shibuya, K., Doi, K., Aoyama, Y. & Hayakawa, H., 2011. Validation of global ocean tide models using the superconducting gravimeter data at Syowa Station, Antarctica, and in situ tide gauge and bottom-pressure observations, *Polar Sci.,* **5,** 21–39.

Kusche, J., 2007. Approximate decorrelation and non-isotropic smoothing of time-variable GRACE-type gravity field models, *J. Geodyn.,* **81,** 733–749.

Landerer, F.W. & Swenson, S.C., 2012. Accuracy of scaled GRACE terrestrial water storage estimates, *Water Resour. Res.,* **48,** W04531, doi:10.1029/2011WR011453.

Lenaerts, J.T.M., van Meijgaard, E., van den Broeke, M.R., Ligtenberg, S.R.M., Horwath, M. & Isaksson, E., 2013. Recent snowfall anomalies in Dronning Maud Land, East Antarctica, in a historical and future climate perspective, *Geophys. Res. Lett.,* **40**(11), 2684–2688.

Nawa, K., Suda, N., Fukao, Y., Sato, T., Aoyama, Y. & Shibuya, K., 1998. Incessant excitation of the Earth's free oscillations, *Earth Planets Space,* **50,** 3–8.

Neumeyer, J., Barthelmes, F., Kroner, C., Petrovic, S., Schmidt, R., Virtanen, H. & Wilmes, H., 2008. Analysis of gravity field variations derived from superconducting gravimeter recordings, the GRACE satellite and hydrological models at selected European sites, *Earth Planets Space,* **60,** 505–518.

Rignot, E., Bamber, J.L., van den Broeke, M.R., Davis, C., Li, Y., van de Berg, W.J. & van Meijgaard, E., 2008. Recent Antarctic ice mass loss from radar interferometry and regional climate modeling, *Nat. Geosci.,* **1,** 106–110.

Rignot, E., Velicogna, I., van den Broeke, M.R., Monaghan, A. & Lenaerts, J., 2011. Acceleration of the contribution of the Greenland and Antarctic ice sheets to sea level rise, *Geophys. Res. Lett.,* **38,** L05503, doi:10.1029/2011GL046583.

Rousseeuw, P.J. & Van Driessen, K., 2006. Computing LTS Regression for Large Data Sets, *Data Min. Knowl. Discovery,* **12**(1), 29–45.

Rye, C.D., Garabato, A.C.N., Holland, P.R., Meredith, M.P., Nurser, A.J.G., Hughes, C.W., Coward, A.C. & Webb, D.J., 2014. Rapid sea-level rise along the Antarctic margins in response to increased glacial discharge, *Nat. Geosci.,* **7,** 732–735.

Sato, T. *et al.*, 1995. One year observations with a superconducting gravimeter at Syowa Station, Antarctica, *J. Geod. Soc. Japan,* **41**(1), 75–89.

Sato, T., Ooe, M., Nawa, K., Shibuya, K., Tamura, Y. & Kaminuma, K., 1997. Long-period tides observed with a superconducting gravimeter at Syowa Station, Antarctica, and their implication to global ocean tide modeling, *Phys. Earth planet. Inter.,* **103**(1–2), 39–53.

Sato, T., Fukuda, Y., Aoyama, Y., McQueend, H., Shibuya, K., Tamura, Y., Asari, K. & Ooe, M., 2001. On the observed annual gravity variation and the effect of sea surface height variations, *Phys. Earth planet. Inter.,* **123,** 45–63.

Shepherd, A. *et al.*, 2012. A reconciled estimate of ice-sheet mass balance, *Science,* **338**(6111), 1183–1189.

Shibuya, K., Doi, K., Fukuzaki, Y. & Iwata, M., 2005. Geodesy reference points within Syowa Station, Antarctica, and their local geodetic ties, *Polar Geosci.,* **18,** 130–161.

Sugawara, Y., 2011. Gravity measurements with the portable absolute gravimeter FG5 at Antarctica (IV), *Bull. Geospat. Info. Authority Japan,* **121,** 9–19 (in Japanese).

Sugiyama, S., Enomoto, H., Fujita, S., Fukui, K., Nakazawa, F., Holmlund, P. & Surdyk, S., 2012. Snow density along the route traversed by the Japanese-Swedish Antarctic Expedition 2007/08, *J. Glaciol.,* **58,** 529–539.

Swenson, S.C., 2012. GRACE monthly land water mass grids NETCDF RELEASE 5.0. Ver. 5.0. PO.DAAC, CA, USA, Dataset accessed [2015-09-10] at: http://dx.doi.org/10.5067/TELND-NC005.

Tamura, Y., 1987. A harmonic development of the tide–generating potential, *Bull. Inf. Marées Terrestres,* **99,** 6813–6855.

Tamura, Y., Sato, T., Ooe, M. & Ishiguro, M., 1991. A procedure for tidal analysis with a Bayesian information criterion, *Geophys. J. Int.,,* **104**(3), 507–516.

Tamura, Y., Aoyama, Y. & Nawa, K., 1997. Gravimetric tidal factors at Syowa Station obtained from three-year observations with a superconducting gravimeter, *Proc. NIPR Symp. Antarct. Geosci.,* **10,** 1–10.

Tapley, B., Bettadpur, S., Ries, J., Thompson, P.F. & Watkins, M., 2004. GRACE measurements of mass variability in the Earth system, *Science,* **305,** 503–505.

Velicogna, I. & Wahr, J., 2006. Measurements of time-variable gravity show mass loss in Antarctica, *Science,* **311,** 1754–1756.

Velicogna, I. & Wahr, J., 2013. Time-variable gravity observations of ice sheet mass balance: precision and limitations of the GRACE satellite data, *Geophys. Res. Lett.,* **40,** 3055–3063.

Wahr, J.M., 1985. Deformation induced by polar motion, *J. geophys. Res.,* **90**(B11), 9363–9368.

Weise, A., Kroner, C., Abe, M., Ihde, J., Jentzsch, G., Naujoks, M., Wilmes, H. & Wziontek, H., 2009. Gravity field variations from superconducting gravimeters for GRACE validation, *J. Geodyn.,* **48,** 325–330.

SUPPORTING INFORMATION

Additional Supporting Information may be found in the online version of this paper:

Figure S1. Weekly status plots of gravity and environmental data: (a) The gravity variation, (b) X tilt power, (c) Y tilt power, (d) the gravity balance signal, (e) atmospheric pressure, (f) the pressure inside dewar. The power spectra of the daily gravity data of 2010 May 12 (g) and 16 (h). A rapid increase in the atmospheric pressure after the blizzard on May 15 affected the pressure inside dewar. Such fluctuation induced the X and Y tilt powers and the gravity fluctuations. The gravity fluctuation occurred at high-frequency bands from 5 to 50 s. Comparing in power spectra between (g) and (h), 1 min interval gravity data were not affected by the rapid increase in the atmospheric pressures.

Figure S2. Topographical maps within a radius of 300 km from SG at Syowa Station. (a) Surface topography (m) based on BEDMAP2 (Fretwell *et al.* 2013) and (b) its elevation angle from SG. Concentric circles with a dashed line indicate distances (km) from SG marked with a cross. Labels of 'A' and 'B' correspond to the areas labelled A and B in Fig. 1(b).
(http://gji.oxfordjournals.org/lookup/suppl/doi:10.1093/gji/ggw078/-/DC1)

Please note: Oxford University Press is not responsible for the content or functionality of any supporting materials supplied by the authors. Any queries (other than missing material) should be directed to the corresponding author for the paper.

APPENDIX: GRAVITY MEASUREMENT WITH THE FIRST-GENERATION SG

The SG is a relative gravimeter utilizing the superconductive phenomenon that occurs at the temperature of LHe (4.2 K), and thus the gravity sensor must be surrounded with LHe continuously. Because the 10 K cryocooler of the TT–70#016 could not liquefy helium gas, LHe was gradually lost through evaporation from the dewar, and needed refilling twice a year as routine maintenance. The operation of helium liquefier and transfer of LHe into the SG dewar significantly disturbed the quality of the gravity data. Fig. A1 shows the time-series of gravity variations obtained with TT-70#016 from March 1993 to January 1998. There are seven significant step–like perturbations (14–502 μGal in magnitude). The step function significantly influences the estimated phase of the periodic gravity variations. If observations were not accompanied by these perturbations, we could confidently analyse the long-period gravity variations. To exclude uncertainty from the long–period analysis, it is useful to use SG data without any such step–like perturbations, even if the data period is short.

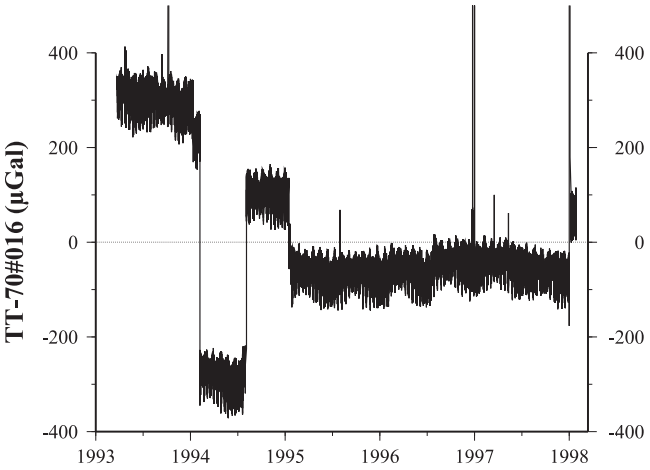

Figure A1. The raw gravity signal obtained from TT–70#016 during 1993–1998. Seven significant step-like perturbations (14–502 (μGal) of magnitude) were caused by electric failures and operation of helium liquefier and transfer of LHe into TT–70#016.